Available online at www.sciencedirect.com
ScienceDirect
International Journal of Heat and Mass Transfer 50 (2007) 1356–1367
International Journal of HEAT and MASS TRANSFER
www.elsevier.com/locate/ijhmt

Linear stability of natural convection in superposed fluid and porous layers: Influence of the interfacial modelling

S.C. Hirata [a], B. Goyeau [a,*], D. Gobin [a], M. Carr [b], R.M. Cotta [c]

[a] Univ. Pierre et Marie Curie, CNRS, Lab. FAST, Bât. 502, Campus Universitaire, F91405 Orsay, France
[b] Division of Civil Engineering, University of Dundee, Dundee DD1 4HN, UK
[c] LTTC/PEM,POLI&COPPE UFRJ Rio de Janeiro, RJ, Brazil

Received 12 June 2006; received in revised form 10 September 2006
Available online 25 January 2007

Abstract

This study deals with the onset of thermal natural convection in a system consisting of a fluid layer overlying a homogeneous porous medium. A linear stability analysis is carried out, using the so-called two-domain approach and including the Brinkman term in the porous region ($2\Omega_{DB}$). Results are systematically compared to those obtained using the one-domain approach (1Ω) and the classical Darcy formulation of the two-domain approach ($2\Omega_{D}$). A better agreement is found between the $2\Omega_{DB}$ and $2\Omega_{D}$ neutral curves, than with the 1Ω curves, indicating that the inclusion of the Brinkman term plays a secondary role on the stability results. The different treatment of the interfacial region is discussed on the basis of these results.

1. Introduction

Convective heat and species transport at the interface between a fluid and a porous region can be encountered in numerous industrial processes (solidification, filtration, catalytic reactor, drying,...) or environmental situations (geothermal systems, ground water pollution,...) and therefore, transport phenomena analysis in such configurations has been the subject of particular attention in the last decades [1]. Nevertheless, one of the fundamental open questions concerns the modelling of the fluid/porous interface and its consequences on transport phenomena. Two different formulations are generally adopted. In the *one-domain approach*, the porous layer is considered as a pseudo fluid and the whole cavity as a continuum [2]. In this case, heat and mass transfer is governed by a unique set of conservation equations valid in both the fluid and porous regions thus avoiding the explicit formulation of boundary conditions at the interface. In the *two-domain approach*, conservation equations in the fluid and in the porous region are coupled by the appropriate set of interfacial conditions. For momentum transport, these conditions mainly depend on the order of the momentum equation in the porous medium whose choice has been widely commented since the pioneering study by Beavers and Joseph [3]. In this study, Beavers and Joseph considered a one-dimensional flow parallel to the fluid/porous interface. Since the flows in the fluid and porous layers are described by the Stokes and Darcy equations, respectively, a semi-empirical slip boundary condition was proposed at the interface

$$\left.\frac{\partial u}{\partial z}\right|_{z=\mathrm{int}} = \frac{\alpha}{\sqrt{K}}\left(u_{\mathrm{int}} - U\right) \tag{1}$$

where u_{int} is the fluid velocity at the interface, U is the seepage velocity, K is the permeability of the homogeneous porous material and α is an *empirical* dimensionless slip coefficient. The agreement between the experimental data provided in [3] and the analytical solution is obtained by adjusting the values of α between 0.1 and 4, depending on the nature of the porous layer. This parameter has been

* Corresponding author. Tel.: +33 1 69 15 80 39.
E-mail address: goyeau@fast.u-psud.fr (B. Goyeau).

0017-9310/$ - see front matter © 2006 Elsevier Ltd. All rights reserved.
doi:10.1016/j.ijheatmasstransfer.2006.09.038

Nomenclature

d_f^*	thickness of the fluid layer, m
d_m^*	thickness of the porous layer, m
d^*	total thickness ($d^* = d_f^* + d_m^*$), m
$\hat{d}$	depth ratio ($\hat{d} = d_f^*/d_m^*$)
Da	Darcy number ($Da = K/d^{*2}$)
g	gravity constant, m s^{-2}
Gr_T	Grashof number ($Gr_T = g\beta_T \Delta T^* d^{*3}/\nu^2$)
K	permeability of the porous medium, m^2
k	thermal conductivity, W m^{-1} K^{-1}
N_θ	truncation order of the temperature expansion
N_W	truncation order of the velocity expansion
Pr	Prandtl number ($Pr = \nu/\alpha_T$)
Ra_T	Rayleigh number ($Ra_T = Gr_T PrDa$)
Ra_{Tf}	fluid Rayleigh number ($Ra_{Tf} = Ra_T/Da$)
Ra_{Tm}	porous Rayleigh number ($Ra_{Tm} = Ra_T \varepsilon_T$)
T_l^*	temperature of the lower boundary, K
T_u^*	temperature of the upper boundary, K

Greek symbols

α	slip coefficient
α_T	thermal diffusivity ($\alpha_{Tf} = k_f/(\rho_0 C_p)_f$, $\alpha_{Tm} = k_m/(\rho_0 C_p)_f$), m^2 s^{-1}
β_T	thermal expansion coefficient, K^{-1}
β_h	temperature eigenvalue
δ	dimensionless parameter ($\delta^2 = (1+\hat{d})^2 Da$)
ε_T	thermal diffusivity ratio ($\varepsilon_T = \alpha_{Tf}/\alpha_{Tm}$)
η	reduced viscosity ($\eta = \mu_{eff}/\mu$)
κ	dimensionless wave number
μ_i	velocity eigenvalue
μ	dynamic viscosity of the fluid, kg m^{-1} s^{-1}
μ_{eff}	effective viscosity of the porous medium, kg m^{-1} s^{-1}
ν	kinematic viscosity of the fluid, m^2 s^{-1}
ρ	fluid density, kg m^{-3}
σ	growth rate
ϕ	porosity
$\tilde{\psi}_{\theta 1}$	temperature eigenfunction for the fluid layer
$\tilde{\psi}_{\theta 2}$	temperature eigenfunction for the porous layer
$\tilde{\psi}_{W1}$	velocity eigenfunction for the fluid layer
$\tilde{\psi}_{W2}$	velocity eigenfunction for the porous layer

Subscripts

0	reference
f	fluid property
m	porous medium property

Superscript

$*$	dimensional quantity

found to be strongly dependent on the structure of the porous interface, but not on the nature of the fluid. Nield [4] was the first to use the slip condition in the stability analysis of superposed fluid and porous layers. Poulikakos et al. [5] also reported a numerical study of high Rayleigh number convection in superposed layers, using the Beavers and Joseph condition. A generalization of the slip condition for multidirectional flows was proposed by Jones [6]. An interesting comparison between the linear stability results obtained using both the Beavers and Joseph and the generalized Jones condition is shown in [7].

An alternative solution to the problem of matching the flow equations in the two regions is to use the Brinkman correction to the Darcy law [8]. Therefore, momentum equations in both regions are of the same differential order and continuity of both velocity and shear stress can be satisfied. In this case, Neale and Nader [9] have shown that the analytical solution is equivalent to the solution of Beavers and Joseph [3] if $\alpha = \sqrt{\mu_{eff}/\mu}$ (μ_{eff} being the effective viscosity involved in the Brinkman term).

Finally, when important spatial variations of the porous structure are present at the fluid/porous inter-region, a macroscopic stress jump boundary condition has been derived in the context of volume averaging [10,11]. This representation, based on the Darcy–Brinkman momentum equation, involves an adjustable stress jump coefficient which has been found to be explicitly dependent on the continuous spatial variations of the effective properties at the inter-region [12,13].

A large majority of studies on linear stability analysis for the onset of thermal convection in superposed fluid and porous layers have been performed using a two-domain approach with the Darcy equation for the momentum transport in the porous region [4,14–17]. The first stability analysis based on the one-domain modelling in this stratified configuration has been proposed by Zhao and Chen [18]. The comparison between their results and those obtained with the two-domain approach [15] shows a qualitative agreement of the marginal stability curves, while the critical values of the Rayleigh number may significantly differ (up to 40%). Up to now, no comparison of the stability results using the two-domain approach and the Darcy–Brinkman formulation in the porous layer was provided.

The only comparison between the one- and two-domain approaches, both including viscous diffusion, have been performed in the context of direct numerical simulations in the configuration studied by Beavers and Joseph [12] or recently for a corner flow [19]. In both cases, it was shown that the two modelling approaches produce similar results. For a corner flow, the finite-element simulations based on the one-domain formulation are also found to be in good agreement with the similarity solution of [20].

The objective of this paper is to develop a linear stability analysis of thermal convection in superposed fluid and homogeneous porous layers using the two-domain Darcy–Brinkman modelling ($2\Omega_{DB}$) and to compare the results obtained with the one-domain approach (1Ω) [21] and the classical Darcy's two-domain formulation ($2\Omega_{D}$) for different slip coefficients [16]. The paper is organized as follows. First, the stability analysis using the two-domain Darcy–Brinkman modelling ($2\Omega_{DB}$) is developed (Sections 2.1 and 2.2). The Generalized Integral Transform Technique (GITT) solution of the eigenvalue problem is detailed in Section 2.3. Then, the stability analysis using the one-domain approach formulation (1Ω) is briefly recalled (Section 3). Finally, the numerical results for the three formulations are compared in Section 4. It is shown that the marginal stability curves for $2\Omega_{DB}$ present a good agreement with those obtained using $2\Omega_{D}$, especially for high α values. For small Darcy values, important discrepancies are found with the 1Ω model. A detailed analysis of the interfacial boundary conditions shows the crucial role of the continuity of normal stress condition on the stability curves.

2. The two-domain approach ($2\Omega_{DB}$)

The system under consideration consists of a horizontal porous layer of thickness d^*_m underlying a fluid layer of thickness d^*_f, with a total thickness $d^* = d^*_m + d^*_f$, as shown in Fig. 1. The upper and lower walls are impermeable and are kept at temperatures T^*_u and T^*_l, respectively. The porous medium is saturated by the same fluid which fills the rest of the domain, and is supposed to be in thermal equilibrium with the fluid. The fluid is assumed to be Newtonian and to satisfy the Boussinesq approximation:

$$\rho(T^*) = \rho_0(1 - \beta_T(T^* - T^*_0)) \tag{2}$$

2.1. Governing equations

Let us now develop the linear stability analysis of thermal convection in the system described above, using the two-domain Darcy–Brinkman modelling. As previously said, the Darcy–Brinkman formulation is different from that of [15,16], since viscous diffusion is included in the momentum equation for the porous medium.

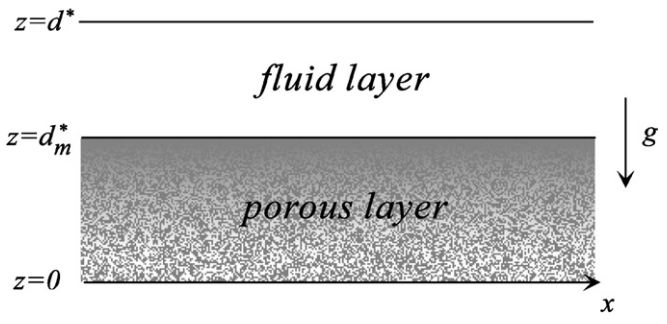

Fig. 1. Geometric configuration of the problem.

The conservation equations for the fluid layer are given by

$$\nabla \cdot \mathbf{u}^* = 0 \tag{3}$$

$$\rho_0\left(\frac{\partial \mathbf{u}^*}{\partial t^*} + (\mathbf{u}^* \cdot \nabla \mathbf{u}^*)\right) = -\nabla P^* + \mu \nabla^2 \mathbf{u}^* - \rho_0 g(1 - \beta_T(T^* - T^*_0))\mathbf{e}_z \tag{4}$$

$$\frac{\partial T^*}{\partial t^*} + \mathbf{u}^* \cdot \nabla T^* = \nabla \cdot (\alpha_{Tf} \nabla T^*) \tag{5}$$

While the equations for the porous layer take the form:

$$\nabla \cdot \mathbf{u}^*_m = 0 \tag{6}$$

$$\frac{\rho_0}{\phi}\frac{\partial \mathbf{u}^*_m}{\partial t^*} = -\nabla P^*_m - \frac{\mu}{K}\mathbf{u}^*_m + \mu_{eff}\nabla^2 \mathbf{u}^*_m - \rho_0 g(1 - \beta_T(T^*_m - T^*_0))\mathbf{e}_z \tag{7}$$

$$\frac{(\rho_0 C_p)_m}{(\rho_0 C_p)_f}\frac{\partial T^*_m}{\partial t^*} + \mathbf{u}^*_m \cdot \nabla T^*_m = \nabla \cdot (\alpha_{Tm} \nabla T^*_m) \tag{8}$$

In Eq. (7), the viscous diffusion term involves the effective viscosity. According to Whitaker [22], the reduced viscosity can be taken as $\eta = \mu_{eff}/\mu = 1/\phi$.

The boundary conditions at the upper boundary $z = d^*$ are: $T^* = T^*_u$, $\mathbf{u}^* = 0$, and at the lower boundary $z = 0$ are: $T^*_m = T^*_l$, $\mathbf{u}^*_m = 0$. At the interface $z = d^*_m$, continuity of temperature, heat flux, velocity, normal stress and tangential stress are imposed:

$$T^* = T^*_m \tag{9}$$

$$k_f \frac{\partial T^*}{\partial z} = k_m \frac{\partial T^*_m}{\partial z} \tag{10}$$

$$\mathbf{u}^* = \mathbf{u}^*_m \tag{11}$$

$$-P^* + 2\mu\frac{\partial w^*}{\partial z} = -P^*_m + 2\mu_{eff}\frac{\partial w^*_m}{\partial z} \tag{12}$$

$$\mu\frac{\partial u^*}{\partial z} = \mu_{eff}\frac{\partial u^*_m}{\partial z} \tag{13}$$

It is important to remark that, when using the Darcy equation, the continuity of normal stress does not include the viscous contribution in the porous region, and the continuity of tangential stress is substituted by the Beavers and Joseph boundary condition (Eq. (1)).

In order to make the equations nondimensional, the following dimensionless variables are introduced: $x = x^*/d^*$, $z = z^*/d^*$, $t = t^*\nu/d^{*2}$, $u = u^*d^*/\nu$, $w = w^*d^*/\nu$, $P = P^*d^{*2}/(\rho_0\nu^2)$, and $T = (T^* - T^*_0)/\Delta T^*$, where $\Delta T^* = T^*_u - T^*_l$. The dimensionless equations for the fluid layer are

$$\nabla \cdot \mathbf{u} = 0 \tag{14}$$

$$\frac{\partial \mathbf{u}}{\partial t} + \mathbf{u} \cdot \nabla \mathbf{u} = -\nabla P + \nabla^2 \mathbf{u} - g\frac{d^3}{\nu^2}(1 - \beta_T(\Delta T^* T))\mathbf{e}_z \tag{15}$$

$$\frac{\partial T}{\partial t} + \mathbf{u} \cdot \nabla T = \frac{1}{Pr_f}\nabla^2 T \tag{16}$$

while assuming that the porous medium is isotropic and homogeneous, the dimensionless equations for the porous layer can be written as

$$\nabla \cdot \mathbf{u}_{\mathrm{m}} = 0 \tag{17}$$

$$\frac{1}{\phi}\frac{\partial \mathbf{u}_{\mathrm{m}}}{\partial t} = -\nabla P_{\mathrm{m}} + \frac{1}{Da}\mathbf{u}_{\mathrm{m}} + \eta\nabla^2\mathbf{u}_{\mathrm{m}} - g\frac{d^3}{\nu^2}(1-\beta_{\mathrm{T}}(\Delta T^* T_{\mathrm{m}}))\mathbf{e}_z \tag{18}$$

$$\frac{(\rho_0 C_p)_{\mathrm{m}}}{(\rho_0 C_p)_{\mathrm{f}}}\frac{\partial T_{\mathrm{m}}}{\partial t} + \mathbf{u}_{\mathrm{m}}\cdot\nabla T_{\mathrm{m}} = \frac{1}{Pr_{\mathrm{m}}}\nabla^2 T_{\mathrm{m}} \tag{19}$$

The nondimensional boundary conditions at the the top and bottom walls are:

$$\begin{aligned} T(1) &= \frac{T_{\mathrm{u}}^* - T_0^*}{\Delta T^*}, \quad \mathbf{u}(1) = 0 \\ T_{\mathrm{m}}(0) &= \frac{T_{\mathrm{l}}^* - T_0^*}{\Delta T^*}, \quad \mathbf{u}_{\mathrm{m}}(0) = 0 \end{aligned} \tag{20}$$

At the interface $z = d_{\mathrm{m}}^*/d^* = d_{\mathrm{m}} = 1/(1+\hat{d})$ the dimensionless boundary conditions take the form:

$$T = T_{\mathrm{m}} \tag{21}$$

$$\frac{\partial T}{\partial z} = \frac{1}{\varepsilon_{\mathrm{T}}}\frac{\partial T_{\mathrm{m}}}{\partial z} \tag{22}$$

$$\mathbf{u} = \mathbf{u}_{\mathrm{m}} \tag{23}$$

$$-P + 2\frac{\partial w}{\partial z} = -P_{\mathrm{m}} + 2\eta\frac{\partial w_{\mathrm{m}}}{\partial z} \tag{24}$$

$$\frac{\partial u}{\partial z} = \eta\frac{\partial u_{\mathrm{m}}}{\partial z} \tag{25}$$

2.2. Linear stability analysis

In order to derive the perturbation equations, we impose perturbations to the basic solution of the dependent variables:

$$\zeta = \overline{\zeta}(z) + \zeta'(x,z,t) \tag{26}$$

where the overlined quantities represent the basic state and the primes denote the perturbation profiles. The steady basic state is supposed to be quiescent: $\bar{u}(z) = \bar{w}(z) = 0$ and $\partial/\partial t = 0$. The equations are linearized in the usual manner.

Using Eq. (26) in Eq. (15), and eliminating the products of perturbed quantities, we obtain for the momentum conservation in the fluid layer:

$$\frac{\partial \mathbf{u}'}{\partial t} = -\nabla(\overline{P} + P') + \nabla^2\mathbf{u}' - g\frac{d^3}{\nu^2}(1-\beta_{\mathrm{T}}\Delta T^*(\overline{T}+T'))\mathbf{e}_z \tag{27}$$

In order to eliminate the pressure term, the above equation is operated with $(\nabla\times\nabla\times)$. Applying continuity, the z-component of Eq. (27) becomes:

$$\left(\frac{\partial}{\partial t} - \nabla^2\right)\nabla^2 w' = Gr_{\mathrm{T}}\nabla_2^2 T' \tag{28}$$

where $\nabla_2^2 = \partial^2/\partial x^2$ in two dimensions and $\nabla_2^2 = \partial^2/\partial x^2 + \partial^2/\partial y^2$ in three dimensions.

Similarly, using Eq. (26) in Eq. (16), and eliminating the products of perturbed quantities gives:

$$\frac{\partial T'}{\partial t} + \frac{\partial \overline{T}}{\partial z}w' = \frac{1}{Pr_{\mathrm{f}}}\nabla^2 T' \tag{29}$$

Eqs. (28) and (29) are the set of perturbation equations for the fluid layer. Proceeding in the same manner, the perturbation equations for the porous layer can be written as

$$\left(\frac{1}{\phi}\frac{\partial}{\partial t} - \eta\nabla^2\right)\nabla^2 w'_{\mathrm{m}} + \frac{1}{Da}\nabla^2 w'_{\mathrm{m}} = Gr_{\mathrm{T}}\nabla_2^2 T'_{\mathrm{m}} \tag{30}$$

$$\frac{(\rho_0 C_p)_{\mathrm{m}}}{(\rho_0 C_p)_{\mathrm{f}}}\frac{\partial T'_{\mathrm{m}}}{\partial t} + \frac{\partial \overline{T}_{\mathrm{m}}}{\partial z}w'_{\mathrm{m}} = \frac{1}{Pr_{\mathrm{m}}}\nabla^2 T'_{\mathrm{m}} \tag{31}$$

The boundary conditions on the external walls are:

$$\begin{aligned} &T'(1) = 0, \quad w'(1) = 0, \quad \frac{\partial w'(1)}{\partial z} = 0, \\ &T'_{\mathrm{m}}(0) = 0, \quad w'_{\mathrm{m}}(0) = 0, \quad \frac{\partial w'_{\mathrm{m}}(0)}{\partial z} = 0. \end{aligned} \tag{32}$$

Making use of the continuity equations for the fluid and the porous regions, the boundary conditions at the interface $z = d_{\mathrm{m}}$ become:

$$T' = T'_{\mathrm{m}} \tag{33}$$

$$\frac{\partial T'}{\partial z} = \frac{1}{\varepsilon_{\mathrm{T}}}\frac{\partial T'_{\mathrm{m}}}{\partial z} \tag{34}$$

$$w' = w'_{\mathrm{m}} \tag{35}$$

$$\frac{\partial w'}{\partial z} = \frac{\partial w'_{\mathrm{m}}}{\partial z} \tag{36}$$

$$(\overline{P} + P') - 2\frac{\partial w'}{\partial z} = (\overline{P}_{\mathrm{m}} + P'_{\mathrm{m}}) - 2\eta\frac{\partial w'_{\mathrm{m}}}{\partial z} \tag{37}$$

$$\frac{\partial^2 w'}{\partial z^2} = \eta\frac{\partial^2 w'_{\mathrm{m}}}{\partial z^2} \tag{38}$$

Let us now apply the normal mode expansion to the dependent variables:

$$(w', T') = (W(z), \theta(z))f(x)\mathrm{e}^{\sigma t} \tag{39}$$

where $\nabla_2^2 f + \kappa^2 f = 0$. The separation constant κ is the nondimensional horizontal wave number. We assume that the principle of exchange of instabilities holds, and the onset of instability is in the form of steady convection ($\sigma = 0$). This assumption was checked in [16] and found to be true in every computational run. Introducing Eq. (39) into Eqs. (28)–(31) gives

$$\frac{\mathrm{d}^4 W}{\mathrm{d}z^4} - 2\kappa^2\frac{\mathrm{d}^2 W}{\mathrm{d}z^2} + \kappa^4 W = \kappa^2 Gr_{\mathrm{T}}\theta \tag{40}$$

$$\frac{\mathrm{d}^2\theta}{\mathrm{d}z^2} - \kappa^2\theta = \frac{1+\hat{d}}{\hat{d}+\varepsilon_{\mathrm{T}}}Pr_{\mathrm{f}}W \tag{41}$$

$$\eta\frac{\mathrm{d}^4 W_{\mathrm{m}}}{\mathrm{d}z^4} - \left(2\eta\kappa^2 + \frac{1}{Da}\right)\frac{\mathrm{d}^2 W_{\mathrm{m}}}{\mathrm{d}z^2} + \left(\eta\kappa^4 + \kappa^2\frac{1}{Da}\right)W_{\mathrm{m}} = \kappa^2 Gr_{\mathrm{T}}\theta_{\mathrm{m}} \tag{42}$$

$$\frac{\mathrm{d}^2\theta_{\mathrm{m}}}{\mathrm{d}z^2} - \kappa^2\theta_{\mathrm{m}} = \varepsilon_{\mathrm{T}}\frac{1+\hat{d}}{\hat{d}+\varepsilon_{\mathrm{T}}}Pr_{\mathrm{m}}W_{\mathrm{m}} \tag{43}$$

The outer boundary conditions take the form

$$\begin{aligned} &\theta(1) = 0, \quad W(1) = 0, \quad \frac{\mathrm{d}W(1)}{\mathrm{d}z} = 0 \\ &\theta_{\mathrm{m}}(0) = 0, \quad W_{\mathrm{m}}(0) = 0, \quad \frac{\mathrm{d}W_{\mathrm{m}}(0)}{\mathrm{d}z} = 0 \end{aligned} \tag{44}$$

while at the interface the boundary conditions can be written as

$$\theta = \theta_{\mathrm{m}} \tag{45}$$

$$\frac{\mathrm{d}\theta}{\mathrm{d}z} = \frac{1}{\varepsilon_{\mathrm{T}}}\frac{\mathrm{d}\theta_{\mathrm{m}}}{\mathrm{d}z} \tag{46}$$

$$W = W_{\mathrm{m}} \tag{47}$$

$$\frac{\mathrm{d}W}{\mathrm{d}z} = \frac{\mathrm{d}W_{\mathrm{m}}}{\mathrm{d}z} \tag{48}$$

$$-\frac{\mathrm{d}^3W}{\mathrm{d}z^3} + 3\kappa^2\frac{\mathrm{d}W}{\mathrm{d}z} = \frac{1}{Da}\frac{\mathrm{d}W_{\mathrm{m}}}{\mathrm{d}z} - \eta\left(\frac{\mathrm{d}^3W_{\mathrm{m}}}{\mathrm{d}z^3} - 3\kappa^2\frac{\mathrm{d}W_{\mathrm{m}}}{\mathrm{d}z}\right) \tag{49}$$

$$\frac{\mathrm{d}^2W}{\mathrm{d}z^2} = \eta\frac{\mathrm{d}^2W_{\mathrm{m}}}{\mathrm{d}z^2} \tag{50}$$

2.3. Solution method – GITT

The system of homogeneous Eqs. (40)–(50) constitutes an eigenvalue problem in Gr_{T}. The GITT [23] solution for this problem is now presented. Following the formalism in this analytic based approach, in particular applied to composite media [24], we choose auxiliary eigenvalue problems for the temperature and velocity fields.

The auxiliary problem for the temperature is:

$$\frac{\mathrm{d}^2\tilde{\psi}_{\theta1,h}(z)}{\mathrm{d}z^2} + \frac{\beta_h^2}{\varepsilon_{\mathrm{T}}}\tilde{\psi}_{\theta1,h}(z) = 0, \quad d_{\mathrm{m}} \leqslant z \leqslant 1 \tag{51}$$

$$\frac{\mathrm{d}^2\tilde{\psi}_{\theta2,h}(z)}{\mathrm{d}z^2} + \beta_h^2\tilde{\psi}_{\theta2,h}(z) = 0, \quad 0 \leqslant z \leqslant d_{\mathrm{m}} \tag{52}$$

where

$$\begin{aligned}&\tilde{\psi}_{\theta1,h}(1) = 0, \quad \tilde{\psi}_{\theta1,h}(d_{\mathrm{m}}) = \tilde{\psi}_{\theta2,h}(d_{\mathrm{m}})\\ &\varepsilon_{\mathrm{T}}\frac{\mathrm{d}\tilde{\psi}_{\theta1,h}(d_{\mathrm{m}})}{\mathrm{d}z} = \frac{\mathrm{d}\tilde{\psi}_{\theta2,h}(d_{\mathrm{m}})}{\mathrm{d}z}, \quad \text{and } \tilde{\psi}_{\theta2,h}(0) = 0\end{aligned} \tag{53}$$

The associated normalized eigenfunctions are:

$$\tilde{\psi}_{\theta1,h}(z) = C_1\frac{\sin\left(\frac{\beta_h}{\sqrt{\varepsilon_{\mathrm{T}}}}(1-z)\right)}{\sin\left(\frac{\beta_h}{\sqrt{\varepsilon_{\mathrm{T}}}}(1-d_{\mathrm{m}})\right)} \tag{54}$$

$$\tilde{\psi}_{\theta2,h}(z) = C_2\frac{\sin(\beta_h z)}{\sin(\beta_h d_{\mathrm{m}})} \tag{55}$$

Boundary conditions (53) provide a system of four linear, homogeneous equations for the determination of the constants C_1 and C_2. Nevertheless, since the resulting system of equations is homogeneous, the constants can be determined only in terms of any of them (i.e., the nonvanishing one) or within a multiple of an arbitrary constant. Therefore, any of the nonvanishing constants can be set equal to unity without loss of generality. Finally, we require that the above system has a nontrivial solution. This condition leads to a transcendental equation for the determination of the eigenvalues β_{h}. The eigenvalue problem (51)–(53) allows the definition of the following integral transform pair:

$$\bar{\theta}_h = \int_{d_{\mathrm{m}}}^{1}\tilde{\psi}_{\theta1,h}(z)\theta_1(z)\mathrm{d}z + \int_0^{d_{\mathrm{m}}}\tilde{\psi}_{\theta2,h}(z)\theta_2(z)\mathrm{d}z \quad \text{(transform)} \tag{56}$$

$$\theta_R(z) = \sum_{h=1}^{\infty}\tilde{\psi}_{\theta R,h}(z)\bar{\theta}_h \quad \text{(inverse)} \tag{57}$$

where $R = 1, 2$ in the fluid and porous regions, respectively. In order to find a group of functions to develop the velocity field, we notice that the usual expansion in terms of trigonometric or Bessel functions is impossible for this problem, since the boundary conditions in the solid walls require that $W = DW = 0$. In this case, the expansion should be in terms of functions which, together with their first derivatives, are null at the limits of the chosen interval. As proposed in [25], the appropriate auxiliary problem is:

$$\frac{\mathrm{d}^4\tilde{\psi}_{W1,i}(z)}{\mathrm{d}z^4} - \mu_i^4\tilde{\psi}_{W1,i}(z) = 0, \quad d_{\mathrm{m}} \leqslant z \leqslant 1 \tag{58}$$

$$\eta\frac{\mathrm{d}^4\tilde{\psi}_{W2,i}(z)}{\mathrm{d}z^4} - \mu_i^4\tilde{\psi}_{W2,i}(z) = 0, \quad 0 \leqslant z \leqslant d_{\mathrm{m}} \tag{59}$$

$$\begin{aligned}&\tilde{\psi}_{W1,i}(1) = 0\\ &\frac{\mathrm{d}\tilde{\psi}_{W1,i}(1)}{\mathrm{d}z} = 0\\ &\tilde{\psi}_{W1,i}(d_{\mathrm{m}}) = \tilde{\psi}_{W2,i}(d_{\mathrm{m}})\\ &\frac{\mathrm{d}\tilde{\psi}_{W1,i}(d_{\mathrm{m}})}{\mathrm{d}z} = \frac{\mathrm{d}\tilde{\psi}_{W2,i}(d_{\mathrm{m}})}{\mathrm{d}z}\\ &\frac{\mathrm{d}^2\tilde{\psi}_{W1,i}(d_{\mathrm{m}})}{\mathrm{d}z^2} = \eta\frac{\mathrm{d}^2\tilde{\psi}_{W2,i}(d_{\mathrm{m}})}{\mathrm{d}z^2}\\ &\frac{\mathrm{d}^3\tilde{\psi}_{W1,i}(d_{\mathrm{m}})}{\mathrm{d}z^3} = \eta\frac{\mathrm{d}^3\tilde{\psi}_{W2,i}(d_{\mathrm{m}})}{\mathrm{d}z^3}\\ &\tilde{\psi}_{W2,i}(0) = 0\\ &\frac{\mathrm{d}\tilde{\psi}_{W2,i}(0)}{\mathrm{d}z} = 0\end{aligned} \tag{60}$$

and the associated normalized eigenfunctions are:

$$\tilde{\psi}_{W1,i}(z) = C_3\mathrm{e}^{-\mu_i z} + C_4\mathrm{e}^{\mu_i z} + C_5\sin(\mu_i z) + C_6\cos(\mu_i z) \tag{61}$$

$$\tilde{\psi}_{W2,i}(z) = C_7\mathrm{e}^{-\frac{\mu_i}{\eta^{1/4}}z} + C_8\mathrm{e}^{\frac{\mu_i}{\eta^{1/4}}z} + C_9\sin\left(-\frac{\mu_i}{\eta^{1/4}}z\right) + C_{10}\cos\left(-\frac{\mu_i}{\eta^{1/4}}z\right) \tag{62}$$

Constants C_3–C_{10} and the eigenvalues μ_i are determined in the same way as in the temperature problem. Following the same procedure, the transformation pair for the momentum problem is defined as

$$\overline{W}_i = \int_{d_{\mathrm{m}}}^{1}\tilde{\psi}_{W1,i}(z)W_1(z)\mathrm{d}z + \int_0^{d_{\mathrm{m}}}\tilde{\psi}_{W2,i}(z)W_2(z)\mathrm{d}z \quad \text{(transform)} \tag{63}$$

$$W_R(z) = \sum_{i=1}^{\infty}\tilde{\psi}_{WR,i}(z)\overline{W}_i \quad \text{(inverse)} \tag{64}$$

The auxiliary eigenvalue problems were chosen in order to satisfy the orthogonality property of the eigenfunctions, which can be written as

$$\int_{d_m}^{1} \tilde{\psi}_{\theta 1,h}(z)\tilde{\psi}_{\theta 1,n}(z)\mathrm{d}z + \int_{0}^{d_m} \tilde{\psi}_{\theta 2,h}(z)\tilde{\psi}_{\theta 2,n}(z)\mathrm{d}z = \delta_{hn}N_h \quad (65)$$

$$\int_{d_m}^{1} \tilde{\psi}_{W1,i}(z)\tilde{\psi}_{W1,j}(z)\mathrm{d}z + \int_{0}^{d_m} \tilde{\psi}_{W2,i}(z)\tilde{\psi}_{W2,j}(z)\mathrm{d}z = \delta_{ij}N_i \quad (66)$$

where δ_{pq} is the Kronecker delta. The normalization integrals are:

$$N_h = \int_{d_m}^{1} \tilde{\psi}^2_{\theta 1,h}(z)\mathrm{d}z + \int_{0}^{d_m} \tilde{\psi}^2_{\theta 2,h}(z)\mathrm{d}z \quad (67)$$

$$N_i = \int_{d_m}^{1} \tilde{\psi}^2_{W1,i}(z)\mathrm{d}z + \int_{0}^{d_m} \tilde{\psi}^2_{W2,i}(z)\mathrm{d}z \quad (68)$$

Eqs. (41) and (43) are operated with $\int_{d_m}^{1} \varepsilon_T \tilde{\psi}_{\theta 1,h}\,\mathrm{d}z$ and $\int_{0}^{d_m} \tilde{\psi}_{\theta 2,h}\,\mathrm{d}z$, respectively. Using Green's theorem, together with boundary conditions (44)–(50) and (53), and the inversion formulae, the following equation is obtained:

$$\begin{aligned}
&\sum_{h=1}^{\infty} \bar{\theta}_h \left(\int_{d_m}^{1} \varepsilon_T \tilde{\psi}_{\theta 1,h} \frac{\mathrm{d}^2 \tilde{\psi}_{\theta 1,n}}{\mathrm{d}z^2}\mathrm{d}z + \int_{0}^{d_m} \tilde{\psi}_{\theta 2,h} \frac{\mathrm{d}^2 \tilde{\psi}_{\theta 2,n}}{\mathrm{d}z^2}\mathrm{d}z \right) \\
&\quad - \kappa^2 \sum_{h=1}^{\infty} \bar{\theta}_h \left(\int_{d_m}^{1} \varepsilon_T \tilde{\psi}_{\theta 1,n}\tilde{\psi}_{\theta 1,h}\mathrm{d}z + \int_{0}^{d_m} \tilde{\psi}_{\theta 2,n}\tilde{\psi}_{\theta 2,h}\mathrm{d}z \right) \\
&\quad = \frac{1+\hat{d}}{\hat{d}+\varepsilon_T} \sum_{i=1}^{\infty} \overline{W}_i \left(Pr_f \int_{d_m}^{1} \varepsilon_T \tilde{\psi}_{\theta 1,n}\tilde{\psi}_{W1,i}\mathrm{d}z \right. \\
&\quad \left. + \varepsilon_T Pr_m \int_{0}^{d_m} \tilde{\psi}_{\theta 2,n}\tilde{\psi}_{W2,i}\,\mathrm{d}z \right)
\end{aligned} \quad (69)$$

Finally, we make use of the auxiliary problem (51) and (52) and apply the orthogonality property (65), to obtain:

$$\begin{aligned}
-\beta_n^2 \bar{\theta}_n &= \kappa^2 \sum_{h=1}^{\infty} \bar{\theta}_h \left(\varepsilon_T \mathscr{J}^{(1)}_{nh} + \mathscr{J}^{(2)}_{nh} \right) \\
&\quad + \frac{1+\hat{d}}{\hat{d}+\varepsilon_T} \varepsilon_T \sum_{i=1}^{\infty} \overline{W}_i \left(Pr_f \mathscr{C}^{(1)}_{ni} + Pr_m \mathscr{C}^{(2)}_{ni} \right)
\end{aligned} \quad (70)$$

where

$$\mathscr{C}^{(R)}_{ni} = \int_R \tilde{\psi}_{\theta R,n}\tilde{\psi}_{WR,i}\,\mathrm{d}z \quad (71)$$

$$\mathscr{J}^{(R)}_{nh} = \int_R \tilde{\psi}_{\theta R,n}\tilde{\psi}_{\theta R,h}\,\mathrm{d}z \quad (72)$$

with $R = 1, 2$.

Following the same procedure, we operate Eqs. (40) and (42) with $\int_{d_m}^{1} \tilde{\psi}_{W1,i}\,\mathrm{d}z$ and $\int_{0}^{d_m} \tilde{\psi}_{W2,i}\,\mathrm{d}z$, respectively. Applying Green's theorem and making use of the inversion formulae, the boundary conditions (44)–(50), (60), the orthogonality property (66), and the auxiliary problems (58) and (59), provide:

$$\begin{aligned}
\mu_i^4 \overline{W}_i &= \sum_{j=1}^{\infty} \overline{W}_j \left(2\kappa^2 \mathscr{F}^{(1)}_{ij} + \left(2\eta\kappa^2 + \frac{1}{Da} \right) \mathscr{F}^{(2)}_{ij} - \kappa^4 \mathscr{E}^{(1)}_{ij} \right. \\
&\quad \left. - \left(\eta\kappa^4 + \kappa^2 \frac{1}{Da} \right) \mathscr{E}^{(2)}_{ij} \right) + \kappa^2 Gr_T \sum_{h=1}^{\infty} \bar{\theta}_h \left(\mathscr{G}^{(1)}_{hi} + \mathscr{G}^{(2)}_{hi} \right) \\
&\quad + \sum_{j=1}^{\infty} \overline{W}_j \left\{ (\kappa^2 - \eta\kappa^2) \tilde{\psi}_{W1,i} \frac{\mathrm{d}\tilde{\psi}_{W1,j}}{\mathrm{d}z} \right. \\
&\quad \left. + \left(2\kappa^2 - 2\eta\kappa^2 - \frac{1}{Da} \right) \tilde{\psi}_{W1,j} \frac{\mathrm{d}\tilde{\psi}_{W1,i}}{\mathrm{d}z} \right\}_{z=dm}
\end{aligned} \quad (73)$$

where

$$\mathscr{E}^{(R)}_{ij} = \int_R \tilde{\psi}_{WR,i}\tilde{\psi}_{WR,j}\,\mathrm{d}z \quad (74)$$

$$\mathscr{F}^{(R)}_{ij} = \int_R \tilde{\psi}_{WR,i} \frac{\mathrm{d}^2 \tilde{\psi}_{WR,j}}{\mathrm{d}z^2}\mathrm{d}z \quad (75)$$

$$\mathscr{G}^{(R)}_{hj} = \int_R \tilde{\psi}_{\theta R,h}\tilde{\psi}_{WR,j}\,\mathrm{d}z \quad (76)$$

with $R = 1, 2$.

In matrix form, the system of Eqs. (70) and (73), can be written as

$$(A_{2\Omega} - Gr_T B_{2\Omega})\,\vec{\tilde{\xi}} = 0 \quad (77)$$

where Gr_T is the eigenvalue, and $\vec{\tilde{\xi}} = \{\overline{W}_1, \overline{W}_2, \ldots, \overline{W}_{N_W}, \bar{\theta}_1, \ldots, \bar{\theta}_{N_\theta}\}$ is the solution vector. It is important to remark that, in order to numerically solve the system, the infinite series were truncated at N_W and N_θ. Matrices $A_{2\Omega}$ and $B_{2\Omega}$ are defined as

$$A_{2\Omega} = \begin{pmatrix} \left(\begin{array}{l} \mu_i^4\delta_{ij} - 2\kappa^2\mathscr{F}^{(1)}_{ij} - (2\eta\kappa^2 + 1/Da)\mathscr{F}^{(2)}_{ij} + \kappa^4\mathscr{E}^{(1)}_{ij} + (\eta\kappa^4 + \kappa^2 1/Da)\mathscr{E}^{(2)}_{ij} \\ \quad \times \left\{ (\kappa^2 - \eta\kappa^2)\tilde{\psi}_{W1,i}\frac{\mathrm{d}\tilde{\psi}_{W1,j}}{\mathrm{d}z} + \left(2\kappa^2 - 2\eta\kappa^2 - \frac{1}{Da}\right)\tilde{\psi}_{W1,j}\frac{d\tilde{\psi}_{W1,i}}{\mathrm{d}z} \right\}_{z=dm} \end{array} \right) & 0 \\ \frac{1+\hat{d}}{\hat{d}+\varepsilon_T}\varepsilon_T \left(Pr_f \mathscr{C}^{(1)}_{nj} + Pr_m \mathscr{C}^{(2)}_{nj} \right) & \beta_n^2\delta_{nh} + \kappa^2 \left(\varepsilon_T \mathscr{J}^{(1)}_{nh} + \mathscr{J}^{(2)}_{nh} \right) \end{pmatrix}$$

and $$B_{2\Omega} = \begin{pmatrix} 0 & \kappa^2 \left(\mathscr{G}^{(1)}_{hi} + \mathscr{G}^{(2)}_{hi} \right) \\ 0 & 0 \end{pmatrix}$$

$A_{2\Omega}$ and $B_{2\Omega}$ are square matrices with $(N_W + N_\theta)$ lines and columns.

3. The one-domain approach (1Ω)

3.1. Governing equations

In this section, we briefly recall the one-domain formulation presented in [21]. This description consists of combining the governing equations for the two regions into a unique set of equations, valid for the entire domain. The momentum conservation equation is a modified Navier–Stokes equation, and thus incorporates the Brinkman extension of Darcy law in the porous medium. As shown in [21], the dimensionless governing equations valid in the two regions are:

$$\nabla \cdot \mathbf{u} = 0 \tag{78}$$

$$\frac{\partial}{\partial t}\left(\frac{\mathbf{u}}{\phi}\right) + \frac{1}{\phi}\left(\mathbf{u}\cdot\nabla\frac{\mathbf{u}}{\phi}\right) = -\nabla P - \frac{1}{Da}\mathbf{u} + \eta\nabla^2\mathbf{u} + (Gr_T T)\mathbf{e}_z \tag{79}$$

$$\frac{(\rho_0 C_p)_m}{(\rho_0 C_p)_f}\frac{\partial T}{\partial t} + \mathbf{u}\cdot\nabla T = \frac{1}{Pr\alpha_{Tf}}\nabla.(\alpha_T\nabla T) \tag{80}$$

where $\alpha_T = \alpha_{Tf}$ in the fluid region and $\alpha_T = \alpha_{Tm}$ in the porous medium. The momentum Eq. (79) continuously evolves from the Darcy–Brinkman equation ($\phi \neq 1$) in the porous region, to the Navier–Stokes equation ($\phi = 1$, $Da \to \infty$) in the fluid region.

3.2. Linear stability analysis

In the linear stability analysis, the final system of perturbation equations for the one-domain approach takes the form:

$$\eta\left(\frac{d^2}{dz^2} - \kappa^2\right)^2 W - \left(\frac{1}{\phi^2}\frac{d\phi}{dz}\right)\frac{d}{dz}\left(\frac{d^2}{dz^2} - \kappa^2\right)W + \frac{1}{Da}\kappa^2 W - \frac{1}{Da}\frac{d^2W}{dz^2} - \frac{d}{dz}\left(\frac{1}{Da}\right)\frac{dW}{dz} - \kappa^2 Gr_T\theta = 0 \tag{81}$$

$$\left(\frac{d^2}{dz^2} + \frac{1}{\alpha_T}\frac{d\alpha_T}{dz}\frac{d}{dz} - \kappa^2\right)\theta = Pr\frac{\alpha_{Tf}}{\alpha_T}W \tag{82}$$

with the following boundary conditions:

$$W = T = \frac{dW}{dz} = 0, \quad \text{at } z = 0, 1 \tag{83}$$

Eqs. (81)–(83) constitutes an eigenvalue problem in Gr_T, for which the GITT solution was presented in detail in [21].

4. Numerical results and discussion

The porous medium is supposed to be isotropic and homogeneous, and in order to compare our results to previous works [15,16,18,21], the parameters Pr, ε_T, and η are fixed at 10, 0.7, and (1/0.39), respectively. After a convergence analysis of the proposed eigenfunction expansion, the truncation order was fixed at $N = N_\theta = N_W = 100$.

The two-domain numerical results are first validated by comparison with the exact values of the Rayleigh–Bénard problem. For a full fluid cavity ($Da \to \infty$, $\phi = 1$), the critical value $Ra_{Tf} = 1707.77$ and the corresponding wave number $\kappa = 3.12$, agree well with the exact values $Ra_{Tf} = 1707.762$ and $\kappa = 3.117$ [26]. For the full porous cavity ($Da = 10^{-5}$, $\hat{d} \to 0$), the results are $Ra_{Tm} = 39.48$ and $\kappa = 3.14$, corresponding to a exact solution of $Ra_{Tm} = 4\pi^2 \approx 39.48$ and $\kappa = \pi \approx 3.14$ [27]. Let us recall that the characteristic parameters obtained with our formulation are the thermal Grashof number Gr_T, and the Darcy number Da. Nevertheless, for the sake of comparison with previous works, the marginal stability curves are presented in terms of the Rayleigh number Ra_T, and according to Chen and Chen [15], the parameter δ is fixed at 0.003. This parameter is actually a combination of Da and the depth ratio $\hat{d}$ ($\delta^2 = (1+\hat{d})^2 Da$).

As already observed by previous authors, the stability curves can present a bimodal behaviour depending on the values of the characteristic parameters. Fig. 2 shows the bimodal nature of the stability curve obtained with the present two-domain Darcy–Brinkman model, for $\hat{d} = 0.12$. Each minimum of the curve correspond to a different mode of natural convection. A "fluid mode" (corresponding to perturbations of large wave numbers), where the convective flow is mainly confined in the fluid layer; and a "porous mode" (corresponding to perturbations of small wave numbers), where the convective flow occurs in the entire porous region. In order to illustrate these two modes, the streamline patterns obtained for $\kappa = 25.5$ and $\kappa = 2.5$ are shown in

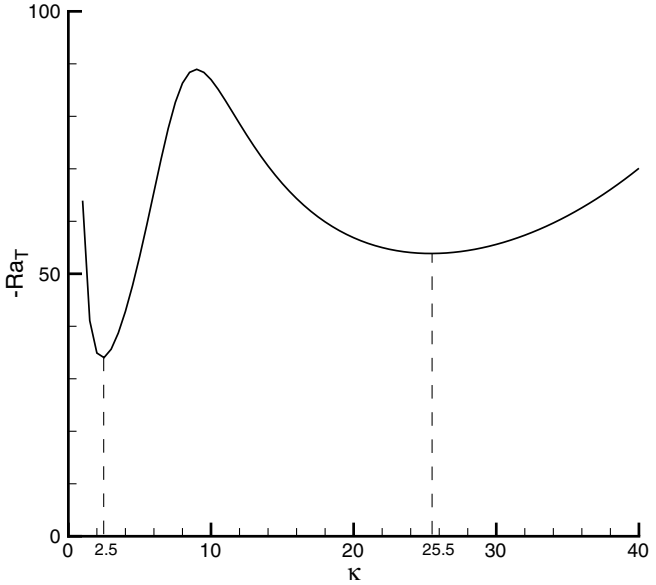

Fig. 2. Bimodal nature of the stability curve obtained with the present $2\Omega_{DB}$ model, for $\hat{d} = 0.12$ and $\delta = 0.003$. The critical values for the first minimum are $-Ra_{Tcr,1} = 34.03$ and $\kappa_{cr,1} = 2.5$; and for the second one, $-Ra_{Tcr,2} = 53.87$ and $\kappa_{cr,2} = 25.5$.

Figs. 3 and 4, respectively. In Fig. 3, a perturbation of large wave number is introduced, resulting in convection cells mainly confined in the fluid layer with some flow penetration in the upper region of the porous layer. Fig. 4 shows the convection pattern obtained for a perturbation of small wave number, corresponding to a large wavelength. In this case, fluid motion is present in the entire porous layer.

Figs. 5–8 show a comparison of the marginal stability curves for four values of $\hat{d}$ at a fixed value of δ ($\delta = 0.003$), obtained with the different models, namely: the one-domain approach (1Ω) [21]; the two-domain approach using Darcy's formulation ($2\Omega_D$) [16] for different values of the adjustable slip coefficient α; and the present two-domain approach using Brinkman's formulation ($2\Omega_{DB}$). Let us remark that the $2\Omega_D$ curves were obtained by Carr and Straughan [16], who adopted a equation of state which expresses the fluid density as a quadratic function of temperature. For all values of $\hat{d}$, it may be noticed that the $2\Omega_{DB}$ curves are located between the curves obtained using the $2\Omega_D$ model, for $\alpha = 1$ and $\alpha = 4$. The stability curves obtained using the 1Ω model present a quite different behaviour. These results show that the Brinkman term does not play a crucial role in the stability of the system for these values of the Darcy number. As a consequence, it may be induced that the discrepancies are due to the different mathematical formulation used in one- and two-domain approaches.

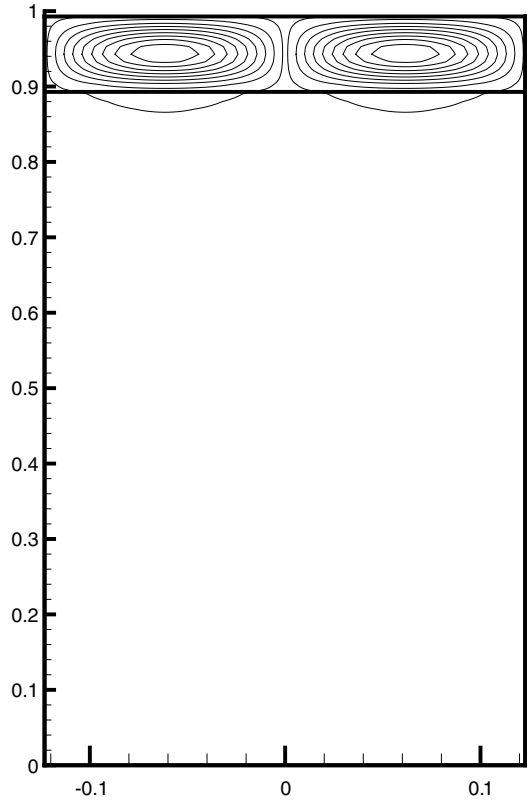

Fig. 3. Streamline patterns at the onset of convection for $\delta = 0.003$, $\hat{d} = 0.12$, and $\kappa = 25.5$, obtained with the $2\Omega_{DB}$ model ($\Psi_{max} = \pm 0.166$; $\Delta\Psi = 0.02$). The thick horizontal line represents the fluid/porous interface.

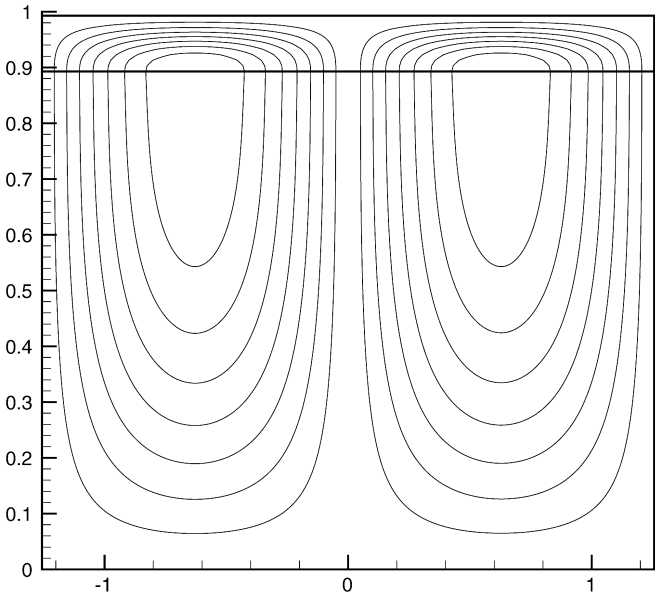

Fig. 4. Streamline patterns at the onset of convection for $\delta = 0.003$, $\hat{d} = 0.12$, and $\kappa = 2.5$, obtained with the $2\Omega_{DB}$ model ($\Psi_{max} = \pm 0.4386$; $\Delta\Psi = 0.0627$). The thick horizontal line represents the fluid/porous interface.

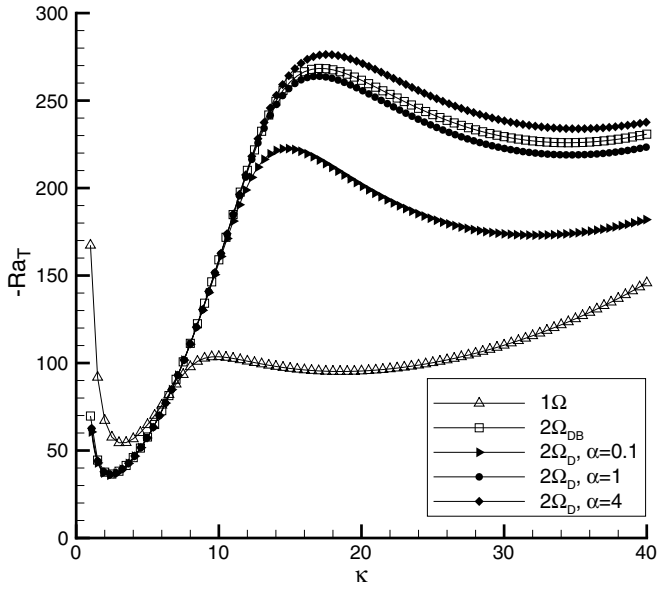

Fig. 5. Marginal stability curves obtained with models 1Ω [21], $2\Omega_D$ [16], and $2\Omega_{DB}$ (present work), for $\hat{d} = 0.08$ and $\delta = 0.003$ (or $Da = 7.72 \times 10^{-6}$).

As shown in [21], our 1Ω curves present a good agreement with the results of Zhao and Chen [18]. In this work, the authors claim a qualitative agreement for the one- and two-domain approaches. Nevertheless, the comparison only concerns the critical values, and not the entire stability curves. They do not mention such important discrepancies

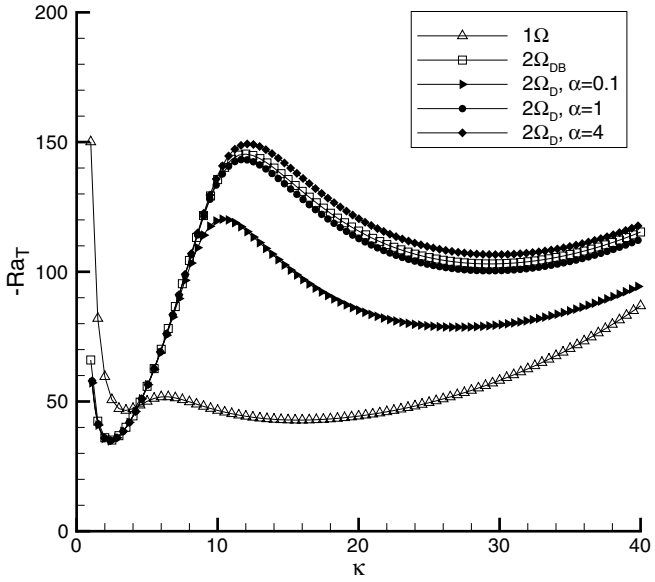

Fig. 6. Marginal stability curves obtained with models 1Ω [21], $2\Omega_D$ [16], and $2\Omega_{DB}$ (present work), for $\hat{d} = 0.10$ and $\delta = 0.003$ (or $Da = 7.44 \times 10^{-6}$).

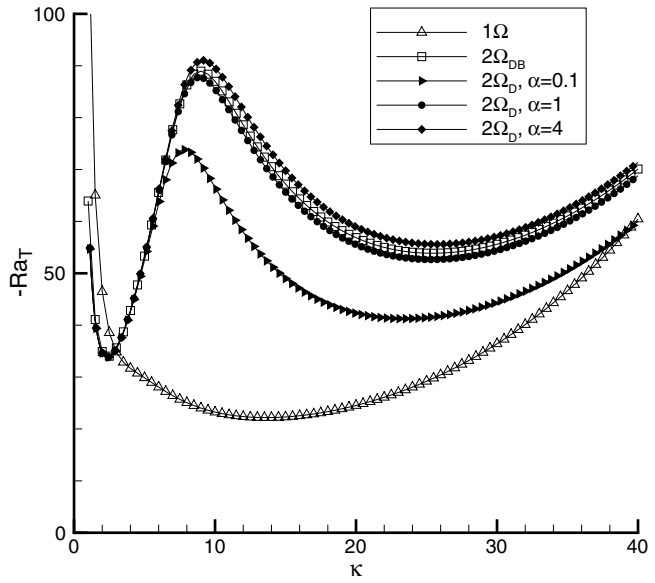

Fig. 7. Marginal stability curves obtained with models 1Ω [21], $2\Omega_D$ [16], and $2\Omega_{DB}$ (present work), for $\hat{d} = 0.12$ and $\delta = 0.003$ (or $Da = 7.17 \times 10^{-6}$).

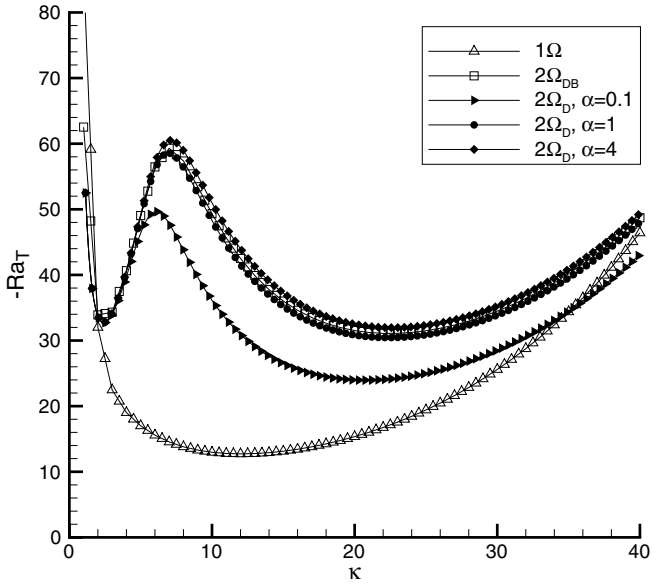

Fig. 8. Marginal stability curves obtained with models 1Ω [21], $2\Omega_D$ [16], and $2\Omega_{DB}$ (present work), for $\hat{d} = 0.14$ and $\delta = 0.003$ (or $Da = 6.93 \times 10^{-6}$).

as those displayed in Figs. 5–8 for large values of κ. The critical Rayleigh numbers and the associated wave numbers for the stability curves in Figs. 5–8 are shown in Table 1. For all values of $\hat{d}$ studied, the $2\Omega_{DB}$ and $2\Omega_D$ curves are bimodal. If one now considers the curves obtained using the 1Ω approach, they also present a bimodal behaviour for $\hat{d} = 0.08$ and $\hat{d} = 0.10$, but not for $\hat{d} = 0.12$ and $\hat{d} = 0.14$, which present only one minimum (Figs. 7 and 8). We can observe an important change in the critical wave number of the 1Ω curves between $\hat{d} = 0.10$ and $\hat{d} = 0.12$ (see Table 1), which corresponds to the change of the critical convection mode. For the $2\Omega_{DB}$ and $2\Omega_D$ curves, the mode switching occurs between $\hat{d} = 0.12$ and $\hat{d} = 0.14$.

The $2\Omega_D$ model requires the specification of the empirical slip parameter α in the Beavers and Joseph boundary condition (Eq. (1)). Contrarily to the findings of Carr and Straughan [16], Chen and Chen [15] mention that their solution "is quite insensitive to α". As shown in Figs. 5–8, this remark is relevant only for small values of the wave number κ, corresponding to the first minimum of the curves. In the $2\Omega_{DB}$ model, on the contrary, there is no adjustable parameter, and therefore only one stability

Table 1
Critical Rayleigh numbers and corresponding wave numbers for the stability curves in Figs. 5–8

Model	$\hat{d} = 0.08$		$\hat{d} = 0.10$		$\hat{d} = 0.12$		$\hat{d} = 0.14$	
	κ_{cr}	$-Ra_{Tcr}$	κ_{cr}	$-Ra_{Tcr}$	κ_{cr}	$-Ra_{Tcr}$	κ_{cr}	$-Ra_{Tcr}$
1Ω	3.0	54.42	3.5	46.55	13.5	22.19	12.0	12.73
$2\Omega_{DB}$	2.5	36.55	2.5	35.15	2.5	34.03	22.0	31.09
$2\Omega_D$, $\alpha = 0.1$	2.4	35.91	2.3	34.81	2.4	33.82	20.5	23.96
$2\Omega_D$, $\alpha = 1$	2.4	36.30	2.4	34.91	2.4	33.81	22.5	30.45
$2\Omega_D$, $\alpha = 4$	2.4	36.37	2.4	34.93	2.4	33.91	22.5	31.96

curve is provided. For the porous mode of instability (first minimum of the curves), all the two-domain curves predict the same critical conditions. This means that when the onset of convective motion occurs within the porous layer, the upper interfacial condition does not play an important role. Concerning the fluid mode of instability, the $2\Omega_{DB}$ curve is systematically located between the $2\Omega_D$ curves for $\alpha = 1$ and $\alpha = 4$. A possible explanation for this fact can be found in the value adopted for the reduced viscosity η. It has been shown that, for one-dimensional flows, the $2\Omega_{DB}$ analytical solution is similar to the $2\Omega_D$ solution by Beavers and Joseph provided that $\alpha = \sqrt{\eta}$ [9]. This is consistent with our results since the porosity of the porous medium ($\phi = 0.39$) is such that $\sqrt{\eta} \cong 1.6$ lies between 1 and 4.

Fig. 9 shows the stability curves obtained with 1Ω and $2\Omega_{DB}$ models, for different values of the Darcy number Da and fixed $\hat{d} = 0.08$. We observe that the models present a better agreement with increasing values of Da. For $Da \geqslant 10^{-4}$, the stability curves present only one minimum, corresponding to the porous convection mode. For $Da = 10^{-5}$, the curves are found to be bimodal, and it can be observed that the 1Ω and $2\Omega_{DB}$ stability curves present larger discrepancies in the region corresponding to the fluid convection mode (large wave numbers). It was verified that for $Da \leqslant 10^{-8}$, there is no penetrating flow, i.e. the porous medium behaves as a solid matrix and convective motion occurs only in the fluid layer.

The fundamental mathematical difference between the one- and two-domain approaches is the treatment of the interface. For this reason, it seems important to analyze the influence of the interfacial boundary conditions. First, instead of imposing the continuity of normal stress, the continuity of pressure was imposed at the interface. Under these circumstances, Eq. (49) is replaced by

$$-\frac{d^3W}{dz^3} + \kappa^2\frac{dW}{dz} = \frac{1}{Da}\frac{dW_m}{dz} - \eta\left(\frac{d^3W_m}{dz^3} - \kappa^2\frac{dW_m}{dz}\right) \quad (84)$$

Eq. (84) differs from Eq. (49) by a factor 3 in the κ^2 terms. The stability curves using the normal stress and the pressure boundary conditions (Eqs. (49) and (84), respectively) are nearly superposed (see Fig. 10), indicating that those terms do not influence the behaviour of the curves and the two boundary conditions are equivalent.

Let us now focus our attention on the first term of the right-hand side of Eq. (49). In order to investigate its influence, it was first assumed $1/Da = 0$ at the interface, i.e.:

$$-\frac{d^3W}{dz^3} + 3\kappa^2\frac{dW}{dz} = -\eta\left(\frac{d^3W_m}{dz^3} - 3\kappa^2\frac{dW_m}{dz}\right) \quad (85)$$

The marginal stability curve obtained using the above boundary condition is also shown in Fig. 10. In fact, it can be observed that the absence of the $\frac{1}{Da}\frac{dW_m}{dz}$ term in the boundary condition significantly influences the behaviour of the stability curve, which becomes very close to the 1Ω curve. This explains why the discrepancies between one- and two-domain models depend not only on the value of Da, but also on the convection mode. Indeed, analyzing the velocity profiles of the fluid and the porous convection modes of the $2\Omega_{DB}$ model (Fig. 11), it can be observed that the vertical velocity gradient at the interface is much greater in the fluid mode. As the velocity gradient multiplies the $1/Da$ term of the normal stress boundary condition, it leads to larger discrepancies of the stability curves on the fluid convection mode.

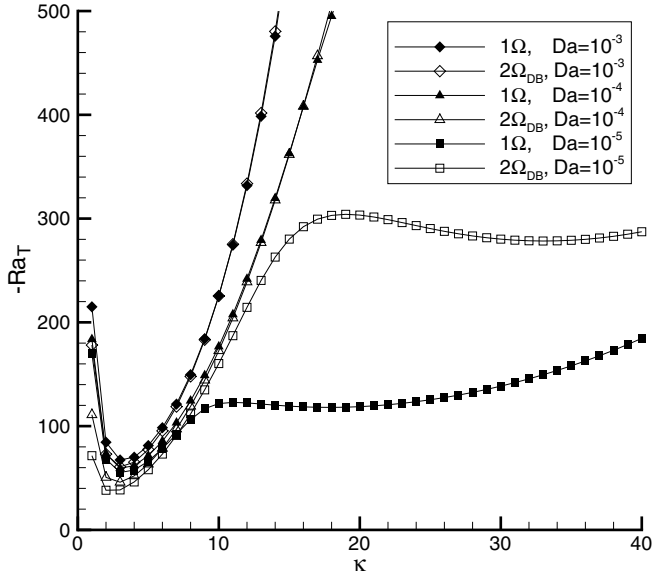

Fig. 9. Marginal stability curves for different values of the Darcy number and $\hat{d} = 0.08$, obtained with models 1Ω [21] and $2\Omega_{DB}$ (present work).

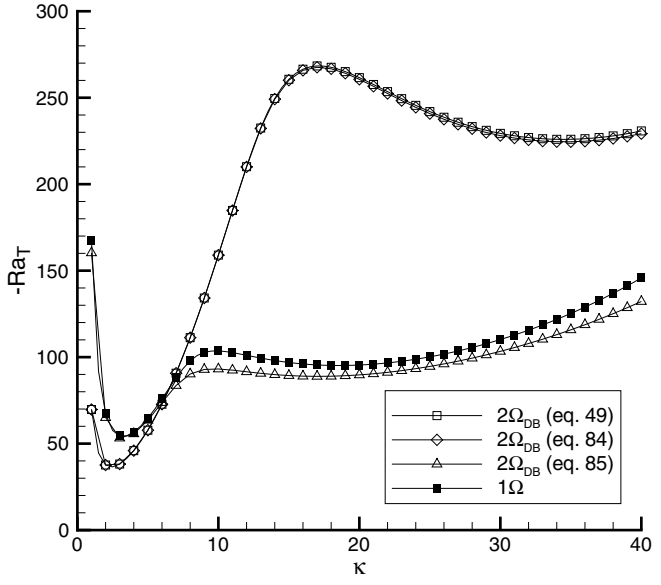

Fig. 10. Comparison of the 1Ω [21] curve with the $2\Omega_{DB}$ curves, for different interfacial conditions (continuity of normal stress – Eq. (49); continuity of pressure – Eq. (84); and assuming $1/Da = 0$ at the interface – Eq. (85)), and $\hat{d} = 0.08$ and $\delta = 0.003$.

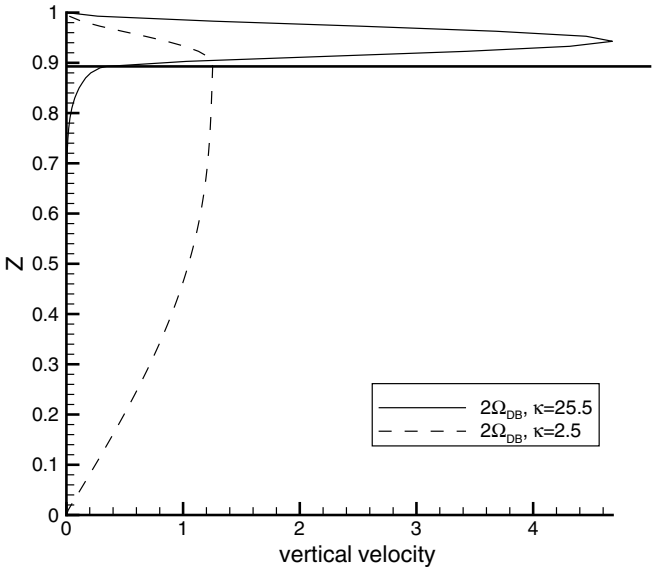

Fig. 11. Vertical velocity profiles for the "fluid" ($\kappa = 25.5$) and the "porous" ($\kappa = 2.5$) convection modes, corresponding to Figs. 3 and 4, respectively. For the fluid mode, $(\partial w/\partial z)_{z=dm} = 24.55$, and for the porous mode, $(\partial w/\partial z)_{z=dm} = 0.0096$. The thick horizontal line represents the fluid/porous interface.

The above conclusion may also explain the fact that some authors [12,20] have found the results of direct simulations of one- and two-domain approaches to be equivalent. Goyeau et al. [12] studied the momentum balance at the interface of a two-layer system, but for a one-dimensional tangential flow (where no normal stress interfacial condition is required). Le Bars and Worster [20] studied the particular case of a corner flow. They imposed continuity of velocities, tangential stress, and pressure across the interface. Nevertheless, the vertical velocity gradient on the interface for this configuration seems to be very small, which would explain the agreement found between one- and two-domain results. The study of bi-dimensional flows of higher intensity seems necessary for the understanding of the differences between one- and two-domain approaches, in the context of direct numerical simulations.

5. Conclusions

A linear stability analysis of thermal natural convection in superposed fluid and porous layers has been carried out, using a Brinkman-extended two-domain model ($2\Omega_{DB}$). The results are compared with those obtained using the classical Darcy's formulation of the two-domain model ($2\Omega_D$) [16], and with the results of the one-domain model (1Ω) [21].

The marginal stability curves of the $2\Omega_{DB}$ model present better agreement with the $2\Omega_D$ curves than with those of the 1Ω approach, indicating that the mathematical formulation has a great influence on the stability results, while the inclusion of the Brinkman term plays a secondary role. The main mathematical aspect responsible for the discrepancies of the marginal stability curves was found to be the different treatment of the interfacial conditions, more specifically in the continuity of normal stress condition. Although this work emphasizes some of the differences between one- and two-domain approaches, the question of the more relevant model still remains open, and more numerical simulations and experiments are needed.

Acknowledgements

This work has been done within the framework of the International Program of Scientific Cooperation (PICS) CNRS-CNPq "Ecoulements et Transferts en Milieux Poreux". SCH gratefully acknowledges the CAPES fellowship (Brazil).

References

[1] D.A. Nield, A. Bejan, Convection in Porous Media, third ed., Springer-Verlag, New York, 2006.
[2] E. Arquis, J.P. Caltagirone, Sur les conditions hydrodynamiques au voisinage d'une interface milieu fluide – milieu poreux: application à la convection naturelle, C. R. Acad. Sci. Paris 299 (1984).
[3] G.S. Beavers, D.D. Joseph, Boundary conditions at a naturally permeable wall, J. Fluid Mech. 30 (1967) 197–207.
[4] D.A. Nield, Onset of convection in a fluid layer overlying a layer of a porous medium, J. Fluid Mech. 81 (1977) 513–522.
[5] D. Poulikakos, A. Bejan, B. Selimos, K.R. Blake, High Rayleigh number in a fluid overlying a porous bed, Int. J. Heat Fluid Flow 7 (1986) 109–116.
[6] I.P. Jones, Low Reynolds number flow past a porous spherical shell, Proc. Camb. Philos. Soc. 73 (1973) 231–238.
[7] M.E. Taslim, U. Narusawa, Thermal stability of horizontally superposed porous and fluid layers, J. Heat Transfer 111 (1989) 357–362.
[8] H.C. Brinkman, A calculation of the viscous force exerted by a flowing fluid on a dense swarm of particles, Appl. Sci. Res. A1 (1947).
[9] G. Neale, W. Nader, Practical significance of Brinkman extention of Darcy's law: coupled parallel flows within a channel and a boundary porous medium, Can. J. Chem. Eng. 52 (1974) 472–478.
[10] J.A. Ochoa-Tapia, S. Whitaker, Momentum transfer at the boundary between a porous medium and a homogeneous fluid – I. Theoretical development, Int. J. Heat Mass Transfer 38 (1995) 2635–2646.
[11] J.A. Ochoa-Tapia, S. Whitaker, Momentum transfer at the boundary between a porous medium and a homogeneous fluid – II. Comparison with experiment, Int. J. Heat Mass Transfer 38 (1995) 2647–2655.
[12] B. Goyeau, D. Lhuillier, D. Gobin, M.G. Velarde, Momentum transport at a fluid–porous interface, Int. J. Heat Mass Transfer 46 (2003) 4071–4081.
[13] M. Chandesris, D. Jamet, Boundary conditions at a planar fluid–porous interface for a poiseuille flow, Int. J. Heat Mass Transfer 49 (13–14) (2006) 2137–2150.
[14] D.A. Nield, The boundary correction for the Rayleigh–Darcy problem: limitations of the Brinkman equation, J. Fluid Mech. 128 (1983) 37–46.
[15] F. Chen, C.F. Chen, Onset of finger convection in a horizontal porous layer underlying a fluid layer, J. Heat Transfer 110 (1988) 403–409.
[16] M. Carr, B. Straughan, Penetrative convection in a fluid overlying a porous layer, Adv. Water Res. 26 (2003) 263–276.
[17] M. Carr, Penetrative convection in a superposed porous-medium-fluid layer via internal heating, J. Fluid Mech. 509 (2004) 305–329.
[18] P. Zhao, C.F. Chen, Stability analysis of double-diffusive convection in superposed fluid and porous layers using a one-equation model, Int. J. Heat Mass Transfer 44 (2001) 4625–4633.

[19] M. Le Bars, M.G. Worster, Solidification of a binary alloy: finite-element, single-domain simulation and new benchmark solutions, J. Comput. Phys. 216 (1) (2006) 247–263.
[20] M. Le Bars, M.G. Worster, Interfacial conditions between a pure fluid and a porous medium: implication for binary alloy solidification, J. Fluid Mech. 550 (2006) 149–173.
[21] S.C. Hirata, B. Goyeau, D. Gobin, R.M. Cotta, Stability of natural convection in superposed fluid and porous layers using integral transforms, Numer. Heat Transfer Part B: Fundam. 50 (5) (2006) 409–424.
[22] S. Whitaker, The Method of Volume Averaging (Theory and Applications of Transport in Porous Media), Springer, 1998.
[23] R.M. Cotta, Integral Transforms in Computational Heat and Fluid Flow, CRC Press, Boca Raton, FL, 1993.
[24] M.D. Mikhailov, M.N. Ozisik, Unified Analysis & Solutions of Heat and Mass Diffusion, John Wiley & Sons, New York, 1984.
[25] M.D. Mikhailov, R.M. Cotta, Integral transform solution of eigenvalue problems, Commun. Numer. Methods Eng. 10 (1994) 827–835.
[26] S. Chandrasekhar, Hydrodynamic and Hydromagnetic Stability, Oxford University Press, 1961.
[27] E.R. Lapwood, Convection of a fluid in a porous medium, Proc. Cambridge Philos. Soc. 44 (1948) 508–521.